Tight Inner Ring Architecture and Quantum Motion of Nuclei Enable Efficient Energy Transfer in Bacterial Light Harvesting

Sohang Kundu[1], Reshmi Dani[1] and Nancy Makri[*1,2,3]

[1]*Department of Chemistry, University of Illinois, Urbana, Illinois 61801*
[2]*Department of Physics, University of Illinois, Urbana, Illinois 61801*
[3]*Illinois Quantum Information Science and Technology Center, University of Illinois, Urbana, Illinois 61801*

* *Email: nmakri@illinois.edu*

Abstract

The efficient, directional transfer of absorbed solar energy between photosynthetic light harvesting complexes continues to pose intriguing questions. In this work we identify the pathways of energy flow between the B800 and B850 rings in the LH2 complex of *Rhodopseudomonas molischianum* using fully quantum mechanical path integral methods to simulate the excited state dynamics of the 24 bacteriochlorophyll molecules and their coupling to 50 normal mode vibrations in each chromophore. While all pigments are identical, the tighter packing of the inner B850 ring is responsible for the thermodynamic stabilization of the inner ring. Molecular vibrations enable the 1 ps flow of energy to the B850 states, which would otherwise be kinetically inaccessible. A classical treatment of the vibrations leads to uniform equilibrium distribution of the excitation, with only 2/3 transferred to the inner ring. However, spontaneous fluctuations associated with the quantum motion of the nuclei increase the transfer efficiency to 90%.

Short title:

Structure and quantum vibrations enable light harvesting

Teaser:

Path integral simulations reveal the mechanistic pathway of inter-ring excitation energy transfer in photosynthetic bacteria

Introduction

Photosynthetic bacteria and plants use optimized arrangements of chromophores and biomolecules, known as light harvesting complexes, to absorb and direct energy with tremendous efficiency towards the reaction center, where charge separation is performed (*1, 2*). The pathways and mechanism of excitation energy transfer (EET) in photosynthetic light harvesting have been the focus of intense experimental and theoretical efforts (*3-6*), motivated in part by the desire to design efficient artificial systems for solar energy harvest and storage.

Understanding EET in light harvesting complexes poses severe challenges due to the quantum mechanical nature of the dynamics and the large number of atoms involved. In this work we focus on the light harvesting complex 2 (LH2) of *Rhodopseudomonas molischianum* (*7*) (Figure 1). The inner B850 ring comprises 16 bacteriochlorophyll (BChl) molecules and is surrounded by the outer B800 ring, which consists of 8 BChl units. The two rings are embedded in a protein and carotenoid environment. Since the computational effort required for solving the Schrödinger equation increases exponentially with system size, accurate simulations of the energy transfer process in these large complexes have been prohibitively demanding. An excellent simplification results from the Frenkel exciton description (*8*), which involves singly excited BChl molecules that are coupled through electronic interactions. In turn, the nuclear degrees of freedom couple to the ground and excited states of each BChl. Within the normal mode approximation, the exciton-vibration couplings are specified in terms of Huang-Rhys factors (*9*). The resulting Hamiltonian (*10*) comprises 24 singly excited electronic states, along with 50 normal modes in each BChl (*11*). Theoretical work on the mechanism of light harvesting has utilized a broad spectrum of available tools, including perturbative Redfield (*12-14*) and Förster approximations (*15-18*), Lindblad master equations (*19, 20*), wavefunction-based methods that include a small number of molecular vibrations (*21-24*), classical trajectory treatments (*25-28*), and fully quantum mechanical methods with simplified vibrational models (*14, 23, 29-31*). However, the intermediate coupling strength and the intricate structure of vibrational environments that characterize nature's energy trapping machinery necessitate the elimination of dynamical approximations and the use of highly structured spectral information.

Numerically exact, fully quantum mechanical methods (*32-36*) based on Feynman's path integral formulation (*37, 38*) of quantum mechanics have enabled accurate simulations of exciton-vibration dynamics in light harvesting complexes (*39-42*), where the coupled electronic states of each molecular unit interact with all intramolecular vibrations within the normal mode approximation. Calculations based on these methods capture the correlated electronic-vibrational motion (*6*) fully quantum mechanically, without resorting to approximations. However, the cost of computing the many-body path integral increases very rapidly with the number of pigments. With recent advances (*43-45*), a simulation of the full two-ring, 24-unit LH2 complex has just become feasible, and the results allow us for the first time to get a reliable glimpse of the pigment-to-pigment energy transfer mechanism within the two-ring complex in full microscopic detail.

Experimental studies suggest that the excitation energy flows inward in the LH2 complex, from the B800 to the B850 ring, in approximately 1 ps at room temperature (*1, 12, 46-49*). (Note that there is considerable agreement among multiple characterization techniques and across different species.) This time is fast compared to the entire light harvesting process (~40 ps) but slow in comparison to the lifetime of electronic coherences (0.1 ps) and the time of energy distribution within the B850 ring (which is comparable to the characteristic time of intramolecular vibrations (*42*)). Further, it is known that energy transfers out

from the B850 ring and to the LH1 complex (within 3 ps) (*1, 47*) before reaching the reaction center (in ~35 ps). Therefore, the inward accumulation of harvested energy in the B850 ring is integral to light harvesting, and decrypting the mechanism of the B800-B850 EET is crucial for understanding photosynthesis and for informing the design of new solar devices.

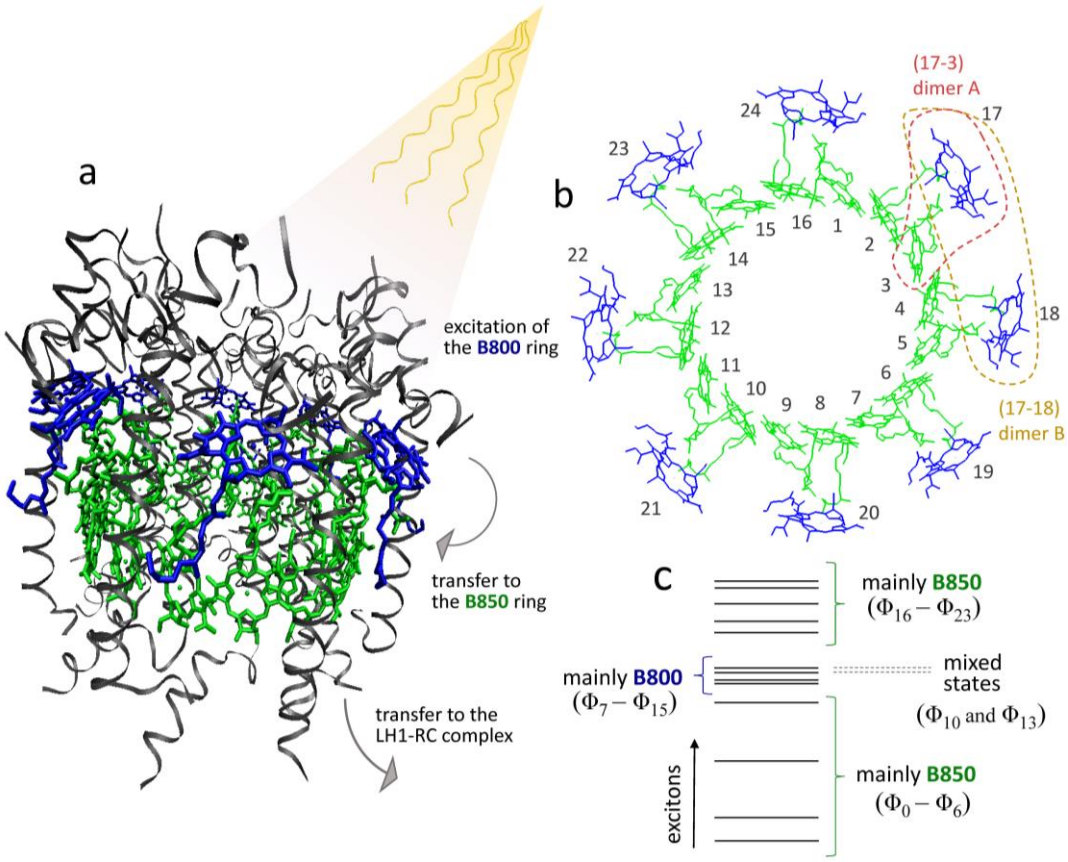

Fig. 1. The biological assembly, structure and energetics. (a) The bacterial LH2 complex in its protein scaffold, (b) the two-ring arrangement of the BChl pigments, and (c) the eigenvalue spectrum of the electronic Hamiltonian. The B800 and B850 rings are shown in blue and green, respectively. Panels a and b include images produced using the Visual Molecular Dynamics (VMD) program (*50*).

In this work we report the mechanistic details of the EET process from an excited BChl of the B800 to the B850 ring (Figure 1a), obtained through fully quantum mechanical calculations based on the single-excitation Frenkel Hamiltonian and a normal mode treatment of all intramolecular vibrations. Electronic parameters are taken from earlier structure calculations (*10*) and the detailed vibrational fine structure of intramolecular Huang-Rhys factors is obtained from fluorescence line narrowing measurements (*11*), augmented with a low-frequency dissipative bath that models the slow motions of the biomolecular environment. Besides reproducing the unidirectional nature and time scale of EET from the B800 to the B850 ring, these simulations allow us to investigate *why* the energy flows towards and becomes trapped

within the inner ring. This is especially perplexing because all BChls are chemically identical and the structure-induced energy differences are much smaller than the thermal energy, such that classical equipartition would predict a uniform equilibrium distribution with only 2/3 of the energy on the B850 ring. In particular, we address the following questions: (i) How does the energy flow from an excited BChl of the B800 ring to the inner ring? (ii) What enables the directional energy transfer and the observed high quantum yield in a complex of identical molecules? The answers we find hold foundational implications for photosynthesis, molecular/materials design, and beyond.

Results

The structure and numbering of the BChl pigments in the LH2 complex are shown in Figure 1b. Each B800 molecule is located between two B850 dimers, but is spatially separated in a different plane. All electronic couplings (*10*) are nonbonded, arising mainly out of dipole interactions, and thus decrease in strength with inter-monomer distance (with the longest-range couplings spanning four monomers). The B850 ring has a tighter spatial arrangement with much stronger excitonic interactions (60-363 cm^{-1}) compared to those in the B800 ring (3-25 cm^{-1}). The interactions between pigments on the two rings are somewhat larger (10-50 cm^{-1}) than those within B800. A small degree of dimerization in the B850 ring gives rise to slightly different intra- and inter-pair excitonic couplings. Further, structural asymmetry in the LH2 complex leads to a small difference (~80 cm^{-1}) in excitation energy that is comparable to or smaller than most of the significant excitonic couplings and the thermal energy at room temperature ($k_{\mathrm{B}}T \sim 200$ cm^{-1}).

The exciton eigenstates are shown in Fig. 1c. The lowest and highest energy eigenstates are composed primarily of B850 BChl excitations, while eigenstates $\Phi_7 - \Phi_{15}$, which form the B800 band, are clustered in the middle. Only two eigenstates (which lie within the B800 band) have significant mixed ring character. The localization of most of the eigenstates on one of the two rings arises from the difference in electronic couplings within B800 and B850, which, in turn, is a consequence of tighter arrangement of the inner ring. We treat the 50 relevant intramolecular vibrations (*11*) of each BChl molecule (1200 total vibrational modes of the complex) explicitly within the normal mode approximation, while the nuclear effects of the surrounding biomolecular environment and the solvent are incorporated using a continuous dissipative bath. Additional details are given in the Supporting Information.

We place the initial excitation on BChl 17 in the B800 ring, while the vibrations remain equilibrated to the electronic ground state at room temperature, in accordance with the Franck-Condon principle. This choice of initial condition allows us to follow the excitation energy as it spreads to other pigments within the complex, and thus is convenient for the purpose of elucidating the mechanism of EET in the LH2 complex. We have recently reported simulations of EET subject to a delocalized excitation of the B800 ring, of the B850 ring, or an excitation that is delocalized over both rings (*51*). The time scales of inter-ring EET transfer resulting from all these initial conditions are identical. The finite-temperature evolution of excitation energy is obtained using a numerically exact, small-matrix decomposition (*43-45*) of the real-time path integral (SMatPI) (see Methods for further details).

The initial excitation on BChl 17 could either spread within the B800 ring (initially to monomers 18, 19 or 23, 24), or it could find its way to the nearby B850 ring (through monomers 1-4), and (since all excited states have approximately the same energy and the coupling between BChl 17 and neighboring pigments have comparable values) both processes are expected to occur simultaneously. To better

understand the relative electronic and electronic-vibrational time scales, we first investigate the EET dynamics within two small subsystems, shown in Fig. 1b: dimer A, comprising one BChl on each ring (monomers 17 and 3, which have identical excitation energies and are coupled by 53 cm^{-1}), and dimer B, which consists of only B800 pigments (identical BChl monomers 17 and 18, coupled by 25 cm^{-1}). Since the two pairs of electronic states in each dimer are resonant, the excitation energy exhibits coherent sinusoidal oscillations in the absence of vibrations (gray lines in Figures 2a and 2b), the characteristic time periods of which depend only on the electronic couplings. Vibrational motion introduces decoherence that quenches the electronic oscillations, and both dimers proceed to thermal equilibrium in ~0.6 and ~4 ps respectively, where the excitation energy is shared equally between the two pigments.

Next, to understand the effects of intra-ring couplings, we examine the specifics of energy redistribution separately within each of the two rings. When the nuclei are frozen, the energy moves coherently among all pigments of the B800 ring. As seen in Fig. 2c, intricate dynamical progressions in the pure electronic dynamics are observed in this larger aggregate, due to the participation of a larger set of eigenstates and hence the introduction of many coherence energy gaps. When the exciton-vibration coupling is included, the population of the initially excited chromophore is seen to decay monotonically within ~8 ps, while all other chromophores rise to the same equilibrium population of 1/8 (as expected, since all monomers are identical).

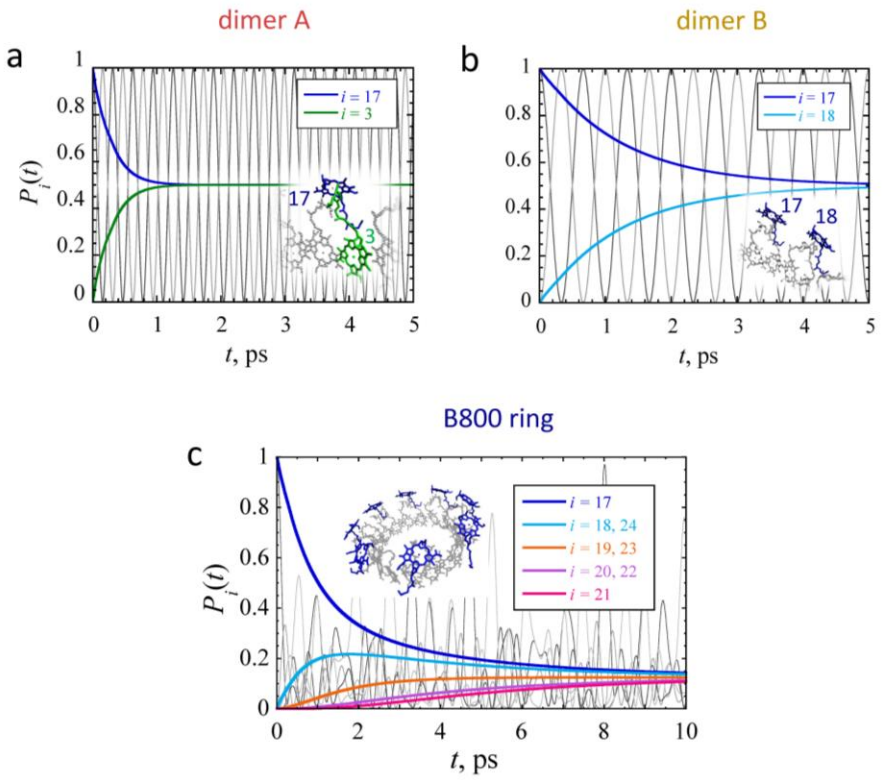

Fig. 2. Pathways of energy transfer in smaller subsystems. Excitation energy transfer in subsystems. (a) Dimer A (pigments 17 and 3). (b) Dimer B (pigments 17 and 18). (c) B800 ring. The gray curves show excited pigment populations in the absence of exciton-vibration coupling.

The BChl vibrations span a large range of frequencies (7-1628 cm^{-1}). Previous work (*42*) used the bath correlation function for the intramolecular spectral density to determine a relevant vibrational time scale of 28 fs. Because of the narrow energy band of the B800 eigenstates (which reflects the weak intra-ring coupling), the electronic time scale is slower by approximately two orders of magnitude (for example, see Fig. 2b). As a result, electronic recurrences are entirely wiped out by the coherence-quenching effects of the vibrational motion, leading to smooth population dynamics. In contrast, minor underdamped and short-lived remnants of electronic oscillations superposed on monotonic decay are observed in similar calculations in the B850 ring alone, where the characteristic time of excitonic couplings is known to be comparable to the intramolecular vibrational time scale (*42*). In that case the excitation was seen to reach a steady state of nearly uniform distribution of population within 0.1 ps.

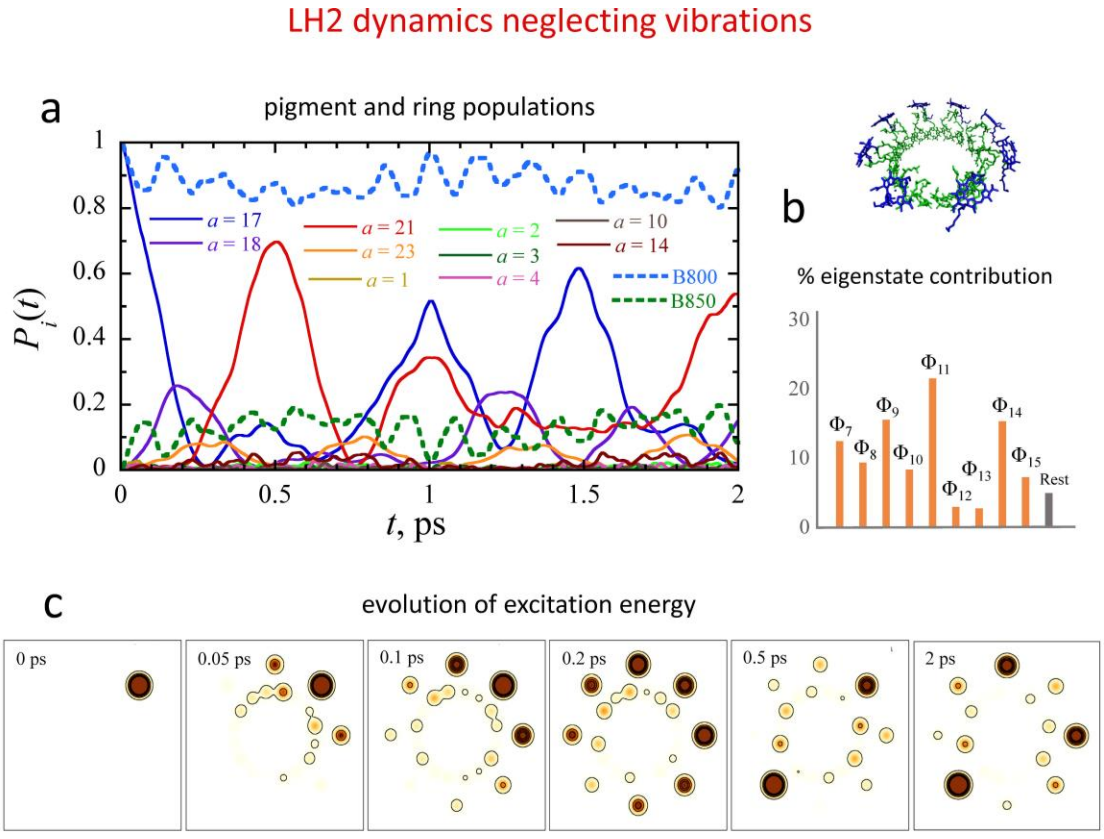

Fig. 3. **Pure exciton dynamics with no nuclear motion.** Population dynamics in the 24-pigment LH2 complex starting with a local excitation in the B800 ring. (a) Population evolution in the absence of vibrations. A representative set of excited state population curves are shown as solid lines. Dashed blue and green lines show the total populations of the two rings. (b) Contribution of the electronic eigenstates to the initial density. (c) Snapshots showing the spatial distribution of excitation energy as a function of time. *Thermodynamic stabilization of the inner ring, enabled by the tight chromophore arrangement, makes it kinetically inaccessible.*

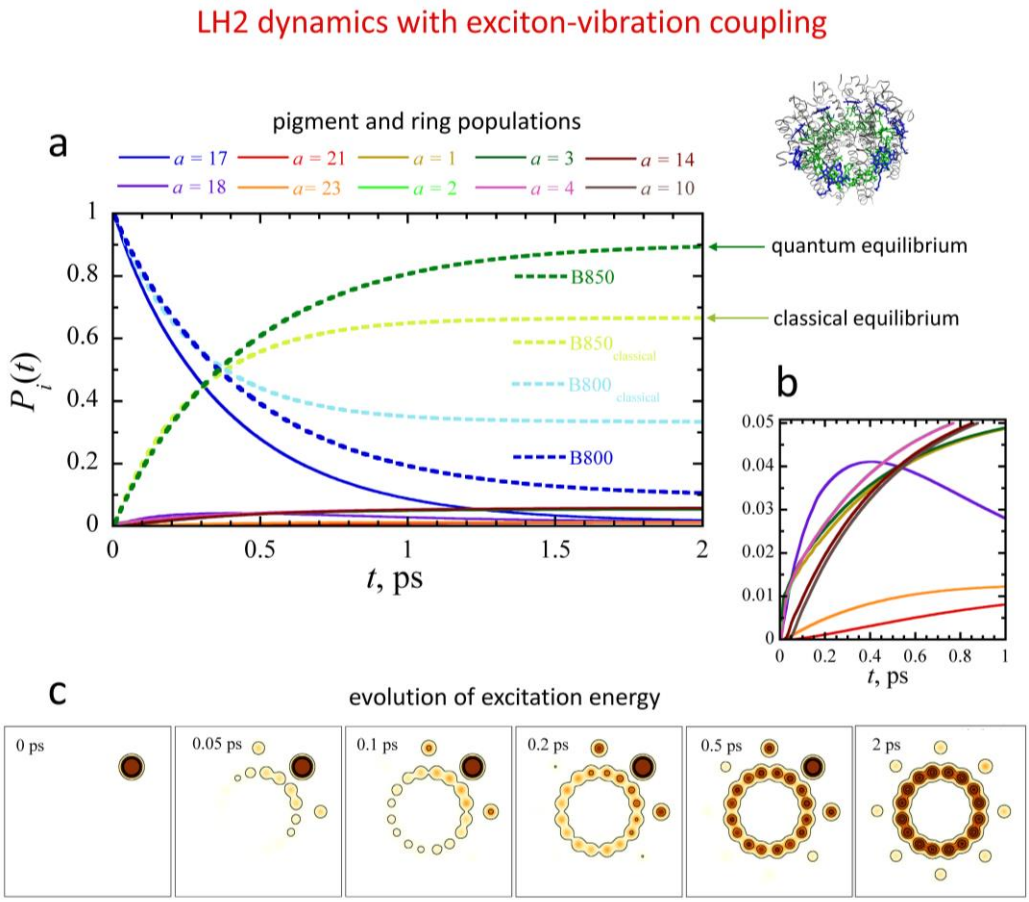

Fig. 4. Excitation energy transfer through the quantum mechanical motion of the nuclei. (a) Population evolution within the 24-unit complex, analogous to Fig. 3a. Again, a representative set of pigment excitations in each ring are shown as solid lines. Dashed blue and green lines show the total populations of the two rings. The dashed cyan and lime lines show the total ring populations obtained from a classical treatment of the nuclei. (b) Enlarged view of the short time transients during excitation transfer. (c) Snapshots showing the spatial distribution of excitation energy as a function of time, analogous to Fig. 3c. *Dynamical fluctuations arising from the quantum mechanical motion of the nuclei enable inward energy transfer.*

We now proceed to the dynamics of the composite two-ring complex with 24 molecular units, subject to the same initial excitation. In sharp contrast to what one would expect based on the complete and rapid transfer of energy to BChl 3 in dimer A within 0.16 ps (which occurs long before transfer to BChl 18 should occur based on dimer B), Figure 3 shows that *almost no energy is transferred to the inner ring in the absence of exciton-vibration coupling*. Instead, the energy is initially transferred to BChl 18 and other neighboring pigments and continues to circulate within the B800 ring, with significant accumulation on the diametrically opposite BChl 21 at 0.5 ps and a large recurrence at 1 ps. Snapshots of population densities (Fig. 3c) taken between 0.05-2 ps after initial excitation also show minor and transient population of pigments of the B850 ring, while the majority of the excitation energy moves around coherently in the outer ring. To understand this behavior, we examine (Fig. 3b) the eigenstate composition of the initially excited

state. Nearly 95% of its population resides on eigenstates $\Phi_7 - \Phi_{15}$, which (as shown in Fig. 1c) have primarily B800 character. Since eigenstate populations cannot change without coupling to vibrational modes, the energy is trapped on the outer ring and cannot access the lower lying states. The two mixed eigenstates Φ_{10} and Φ_{13} of the central band share moderate contributions from B850 pigments and their small overlaps with the initially excited state contribute to the observed weak oscillatory population transfer.

The quantum mechanical motion of the nuclei enables population transfer to lower-lying eigenstates through exciton-vibration coupling and leads to the unidirectional flow of energy from the B800 to the B850 ring (Figure 4). While energy transfer to nearby pigments on both rings appears equally likely based on local energetics, and in contrast to the EET pathway observed in the absence of exciton-vibration coupling, only a small (<0.04) transient accumulation of energy on BChl 18 and 24 is now observed. This transient population is rapidly depleted to B850 pigments, while the remaining B00 pigments are minimally populated. The stronger intra-B850 coupling leads to the very rapid (~0.1 ps) redistribution of energy within the inner ring, thereby disfavoring the spread of the excitation to other B800 pigments. The continued siphon-like leakage of excitation energy from BChl 17 leads to the steady increase of population of the entire B850 ring, which follows an exponential curve with a 1/e time of 0.43 ps, and the energy transfer is nearly complete within 1 ps. The rate obtained from the path integral calculations is in good agreement with the experimental value of 1.08 ps (*49*). Further, the total ring population curves are nearly identical to those obtained with eigenstate initial conditions (*51*). Snapshots and molecular illustrations of excited pigment populations are shown in Fig. 4c and Figure 5, respectively.

Discussion

From the perspective of energetics, the early transfer of excitation to pigments 1-3 is favored because these pigments belong to eigenstates of lower energy that are delocalized over the B850 ring. As discussed earlier, half of the B850 eigenstates lie lower than the B800 states because of the larger electronic couplings between BChl units of the tightly packed inner ring. The resulting energy bias, which favors the B850 ring *thermodynamically*, also makes the B850 pigments *kinetically* inaccessible from states of the B800 band, leading to the spreading of energy only around the B800 ring observed in the absence of exciton-vibration coupling (Fig. 3). Vibrational motion introduces fluctuations that modulate electronic energy gaps, activating the downhill energy flow pathway to the inner ring. Thus, *the tight architecture of the inner ring creates the necessary thermodynamic condition for nearly complete inward energy transfer, while the motion of the nuclei is responsible for making this transfer kinetically feasible.*

If the nuclei were to move classically without properly responding to the quantum transitions that underlie the EET dynamics, level fluctuations would still enable the transfer of energy to the inner ring, but with reduced efficiency. This is because the electronic Hamiltonian is symmetric with respect to the coupling between states, such that a difference between “up” and “down” rates arises exclusively from the “back reaction”, i.e. the change of course the nuclei should incur following each electronic transition (*52*), which produces a subtle, purely quantum mechanical phase related to vacuum fluctuations (*53*). This quantum phase contributes an imaginary component to the energy gap correlation function (which gives the exponent of the influence functional within the path integral formulation (*52, 54*) and also appears in the Redfield (*55*) and Förster (*56*) approximations) that enables the *spontaneous* emission of electronic energy quanta to the vibrational bath, an entirely quantum mechanical decoherence process which leads to

populations that satisfy the detailed balance property (with respect to the full electronic-vibrational Hamiltonian) in the long-time limit. The neglect of the vacuum phase (which is necessary in many crude quantum-classical treatments of nonadiabatic dynamics) allows "up" and "down" electronic transitions with equal probabilities. We note that the addition of zero-point energy effects to the motion of the nuclei by itself does not cure the shortcomings associated with the neglect of the strictly quantum mechanical pathway of energy transfer through the vacuum phase.

In the case of the LH2 complex, results obtained with a fully classical treatment of the nuclei (which does not account for the vacuum phase) lead to faster transfer, with a 1/e time of 0.28 fs, and a uniform distribution of excitation energy among all BChl molecules according to the classical equipartition principle, such that only 16/24 = 67% of the energy resides on the B850 ring at equilibrium. The resulting dynamical process is shown in Fig. 4. Similar conclusions regarding equilibration to incorrect values upon neglecting the imaginary vacuum phase in perturbative treatments have been reported in other recent works as well (*5, 57*). Thus, the high efficiency of 90% energy transfer to the inner ring is enabled exclusively through the additional *quantum decoherence* pathway that gives rise to *spontaneous* emission of excitation energy and its preferential accumulation on the lower-lying B850 states, which is orchestrated by the quantum mechanical motion of the nuclei. Thus, the latter is crucial for enhancing the efficiency of photosynthetic light harvesting from moderate (67%) to excellent (>90%).

While being limited by intrinsic assumptions and unable to offer detailed dynamical information, perturbative treatments can provide valuable rate estimates in situations where full simulation is prohibitively expensive. Generalized Förster theory (*15-18, 58, 59*) (GFT) is applicable to the LH2 dynamics by reducing the B800 ring to a single monomer that is weakly coupled to the BChl molecules of the B850 ring. An important advantage of GFT is the expression of the energy transfer rate in terms of the overlaps between absorption and emission spectra, which often are available from experiments. To test the validity of a perturbative rate approximation by comparing against the accurate path integral results obtained for the same electronic coupling parameters and spectral density, we have calculated the GFT rate for the LH2 complex of *Rhodopseudomonas molischianum*, approximating the absorption lineshape of the B850 ring by that of a single BChl molecule in order to maintain simplicity and avoid the need for dipole moment vector information. The resulting GFT rate corresponds to a 1/e time of ~0.46 ps, which is in excellent agreement with the ~0.43 ps time obtained from the path integral simulations.

We therefore establish that photosynthesis utilizes differences in ring architecture and the packing of pigments, as well as the quantum mechanical motion of the nuclei, to efficiently channel the flow of absorbed energy through biomolecular complexes. The tighter ring architecture of the inner ring creates differences between the inter-ring and intra-ring pathways. In the absence of vibrations, this difference in excitonic couplings would localize the excited energy in the outer ring, disabling the required transfer of energy to the B850 ring (and hence to the LH1 and the reaction center). On the other hand, decoherence through the motion of the nuclei completely alters the energy transfer pathways. 67% of the excitation is transferred and equilibrates from entirely classical fluctuations giving rise to stimulated exciton-vibration energy exchange, while purely quantum mechanical processes associated with vacuum fluctuations enable spontaneous emission that effectively moves additional energy out of the higher-lying states of the outer ring, trapping 90% of the excitation energy on B850 pigments. Thus, the tight inner ring architecture and the quantum motion of the nuclei are indispensable components of nature's design that allows efficient, unidirectional energy transfer in bacterial light harvesting.

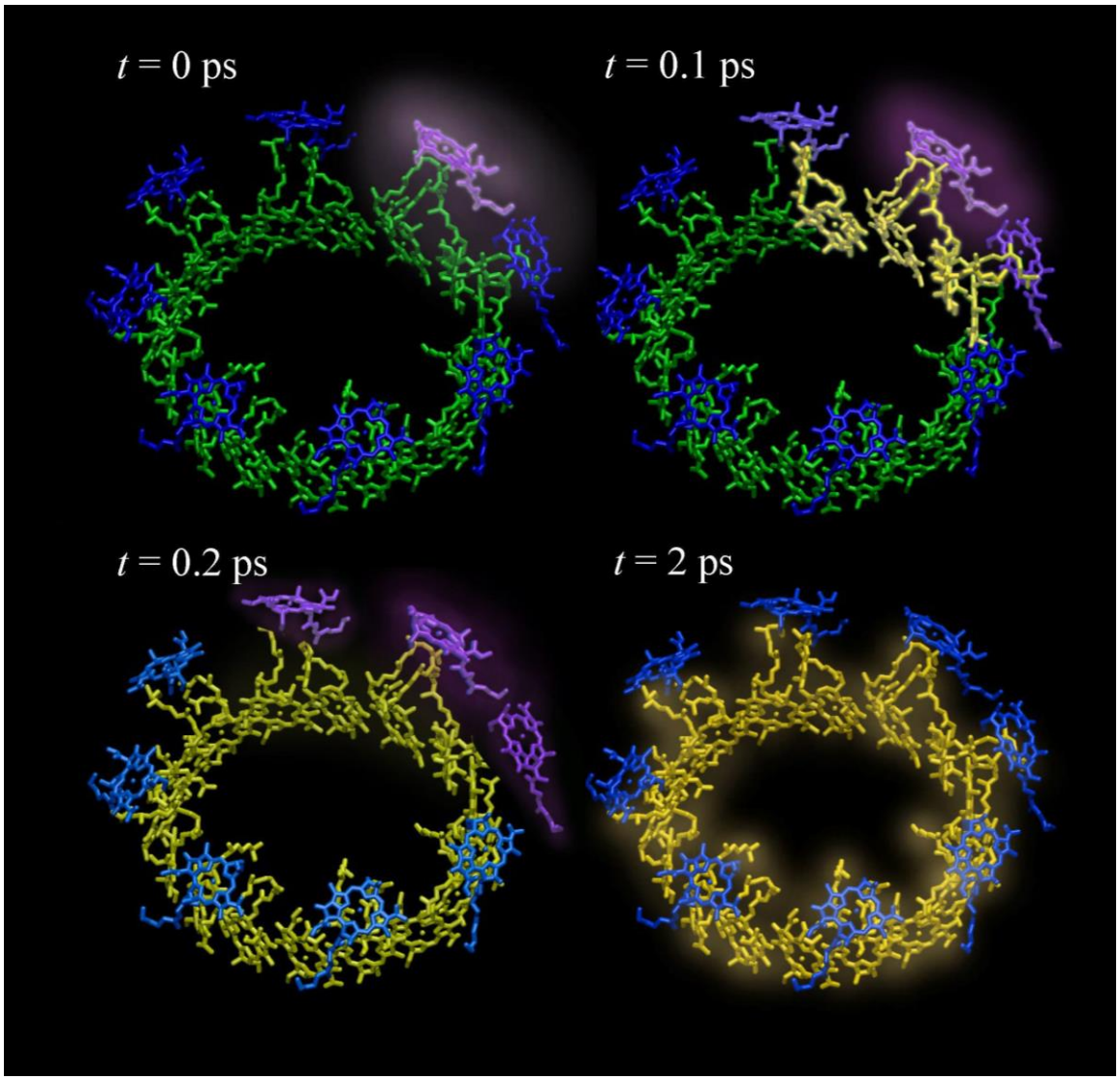

Fig. 5. Illustration of the EET pathway in the LH2 complex. Following an initial excitation of the B800 ring, the nuclear vibrational motion *kinetically enables the spread of the excitation to the B850 ring, which is thermodynamically favored at equilibrium because of the tight pigment packing*. A minor spread of excitation energy to the nearest neighbor pigments is initially observed, which rapidly spreads to the B850 ring. The process continues until 90% of the excitation resides on inner ring pigments.

Methods

Hamiltonian and initial conditions. The Hamiltonian for a BChl monomer consists of a ground and an excited electronic state. Earlier work based on fluorescence experiments has identified 50 coupled normal mode vibrations that couple to the electronic states and reported the corresponding Huang-Rhys factors

(*11*). In addition to the discrete vibrational modes, a low-frequency component that models the protein and solvent environment is added to the spectral density.

The parameters of the electronic Hamiltonian are obtained from earlier electronic structure calculations (*60*). It is assumed that the initial excitation is localized on a single monomer. All vibrational modes are equilibrated to the electronic ground state of each monomer, in accordance with the Franck-Condon principle.

Quantum dynamics. The time evolution of the excited state populations is performed using the small matrix decomposition of the path integral (*43-45*) (SMatPI) in the quasi-adiabatic propagator (*32, 33, 61*) (QuAPI) representation, which is a numerically exact, fully quantum mechanical method for simulating the dynamics of a system coupled to an environment consisting of harmonic degrees of freedom. The path integral is discretized on a time grid using the QuAPI factorization of the propagator and the harmonic degrees of freedom are integrated out analytically at the desired temperature, giving rise to a QuAPI-discretized (*62*) influence functional (*63*). The time evolution of the reduced density matrix is calculated through a series of $n^2 \times n^2$ matrix operations, where n is the number of electronic states.

Acknowledgements:

We thank Gregory D. Scholes and Graham R. Fleming for useful correspondence regarding the calculation of GFT rates.

Funding: This material is based upon work supported by the National Science Foundation under Award CHE-1955302. Some of this research is part of the Blue Waters sustained-petascale computing project, which is supported by the National Science Foundation (Awards OCI-0725070 and ACI-1238993) and the state of Illinois. Blue Waters is a joint effort of the University of Illinois at Urbana-Champaign and its National Center for Supercomputing Applications.

Author contributions: N.M. and S.K. designed the project. S.K. and R.D. performed the calculations. S.K. and N.M. carried out the analysis and wrote the paper. All authors contributed to the figures and the final editing of the paper.

Competing Interests: The authors declare that they have no competing interests.

Data availability: All data needed to evaluate the conclusions in the paper are present in the paper and/or the Supplementary Materials.

References

1. T. Pullerits, V. Sundstrom, Photosynthetic light-harvesting pigment-protein complexes: Toward understanding how and why. *Acc. Chem. Res.* **29**, 381-389 (1996).
2. R. E. Blankenship, *Molecular mechanisms of photosynthesis*. (World Scientific, London, 2002).
3. A. Ishizaki, G. R. Fleming, Quantum Coherence in Photosynthetic Light Harvesting. *Annual Review of Condensed Matter Physics* **3**, 333-361 (2012).
4. A. Chenu, G. D. Scholes, Coherence in Energy Transfer and Photosynthesis. *Annual Review of Physical Chemistry* **66**, 69-96 (2015).
5. J. Cao *et al.*, Quantum biology revisited. *Science Advances* **6**, eaaz4888 (2020).
6. S. Kundu, N. Makri, Intramolecular Vibrations in Excitation Energy Transfer: Insights from Real-Time Path Integral Calculations. *Annual Review of Physical Chemistry* **73**, 349-375 (2022).
7. J. Koepke, X. Hu, C. Muenke, K. Schulten, H. Michel, The crystal structure of the light harvesting complex II (B800-B850) from Rhodospirillum molischianum. *Structures* **4**, 581-597 (1996).
8. J. Frenkel, On the transfomation of light into heat in solids. *Phys. Rev.* **37**, 17 (1931).
9. K. Huang, A. Rhys, Theory of light absorption and non-radiative transitions in F-centres. *Proceedings of the Royal Society of London. Series A. Mathematical and Physical Sciences* **204**, 406-423 (1950).
10. S. Tretiak, C. Middleton, V. Chernyak, S. Mukamel, Bacteriochlorophyll and carotenoid excitonic couplings in the LH2 system of purple bacteria. *J. Phys. Chem. B* **104**, 9540-9553 (2000).
11. M. Rätsep, Z.-L. Cai, J. R. Reimers, A. Freiberg, Demonstration and interpretation of significant asymmetry in the low-resolution and high-resolution Qy fluorescence and absorption spectra of bacteriochlorophyll a. *J. Chem. Phys.* **134**, 024506 (2011).
12. V. Sundstrom, T. Pullerits, R. van Grondelle, Photosynthetic light harvesting: Reconciling dynamics and structure of purple bacterial LH2 reveals function of photosynthetic unit. *J. Phys. Chem. B* **103**, 2327-2346 (1999).
13. J. Adolphs, T. Renger, How proteins trigger excitation energy transfer in the FMO complex of green sulfur bacteria. *Biophys J.* **91**, 2778–2797 (2006).
14. A. Ishizaki, G. R. Fleming, On the adequacy of the Redfield equation and related approaches to the study of quantum dynamics in electronic energy transfer. *The Journal of Chemical Physics* **130**, 234110 (2009).
15. K. Mukai, S. Abe, H. Sumi, Theory of Rapid Excitation-Energy Transfer from B800 to Optically-Forbidden Exciton States of B850 in the Antenna System LH2 of Photosynthetic Purple Bacteria. *The Journal of Physical Chemistry B* **103**, 6096-6102 (1999).
16. G. D. Scholes, G. R. Fleming, On the Mechanism of Light Harvesting in Photosynthetic Purple Bacteria: B800 to B850 Energy Transfer. *The Journal of Physical Chemistry B* **104**, 1854-1868 (2000).
17. S. Jang, M. D. Newton, R. J. Silbey, Multichromophoric Förster Resonance Energy Transfer from B800 to B850 in the Light Harvesting Complex 2: Evidence for Subtle Energetic Optimization by Purple Bacteria. *The Journal of Physical Chemistry B* **111**, 6807-6814 (2007).
18. T. Mirkovic *et al.*, Light Absorption and Energy Transfer in the Antenna Complexes of Photosynthetic Organisms. *Chemical Reviews* **117**, 249-293 (2017).
19. B. Palmieri, D. Abramavicius, S. Mukamel, Lindblad equations for strongly coupled populations and coherences in photosynthetic complexes. *The Journal of Chemical Physics* **130**, 204512 (2009).
20. D. Abramavicius, S. Mukamel, Energy-transfer and charge-separation pathways in the reaction center of photosystem II revealed by coherent two-dimensional optical spectroscopy. *The Journal of Chemical Physics* **133**, 184501 (2010).

21. V. Tiwari, W. K. Peters, D. M. Jonas, Electronic resonance with anticorrelated pigment vibrations drives photosynthetic energy transfer outside the adiabatic framework. *Proc. Nat. Acad Sci. USA* **110**, 1203-1208 (2013).
22. M. Schröter *et al.*, Exciton–vibrational coupling in the dynamics and spectroscopy of Frenkel excitons in molecular aggregates. *Physics Reports* **567**, 1-78 (2015).
23. S.-H. Yeh, R. D. Hoehn, M. A. Allodi, G. S. Engel, S. Kais, Elucidation of near-resonance vibronic coherence lifetimes by nonadiabatic electronic-vibrational state character mixing. *Proceedings of the National Academy of Sciences* **116**, 18263-18268 (2019).
24. P. Bhattacharyya, G. R. Fleming, Two-Dimensional Electronic–Vibrational Spectroscopy of Coupled Molecular Complexes: A Near-Analytical Approach. *The Journal of Physical Chemistry Letters* **10**, 2081-2089 (2019).
25. W. H. Miller, Electronically nonadiabatic dynamics via semiclassical initial value methods. *J. Phys. Chem.* **113**, 1405-1415 (2009).
26. G. Tao, W. H. Miller, Semiclassical description of electronic excitation population transfer in a model photosynthetic system. *J. Phys. Chem. Lett.* **1**, 891-894 (2010).
27. P. Huo, D. F. Coker, Iterative linearized density matrix propagation for modeling coherent excitation energy transfer in photosynthetic light harvesting. *J. Chem. Phys.* **133**, 184108 (2010).
28. A. Sisto *et al.*, Atomistic non-adiabatic dynamics of the LH2 complex with a GPU-accelerated ab initio exciton model. *Physical Chemistry Chemical Physics* **19**, 14924-14936 (2017).
29. A. Ishizaki, G. R. Fleming, Theoretical examination of quantum coherence in a photosynthetic system at physiological temperature. *Proceedings of the National Academy of Sciences* **106**, 17255-17260 (2009).
30. C. Kreisbeck, T. Kramer, A. Aspuru-Guzik, Scalable High-Performance Algorithm for the Simulation of Exciton Dynamics. Application to the Light-Harvesting Complex II in the Presence of Resonant Vibrational Modes. *Journal of Chemical Theory and Computation* **10**, 4045-4054 (2014).
31. H. C. H. Chan, O. E. Gamel, G. R. Fleming, K. B. Whaley, Single-photon absorption by single photosynthetic light-harvesting complexes. *Journal of Physics B: Atomic, Molecular and Optical Physics* **51**, 054002 (2018).
32. N. Makri, D. E. Makarov, Tensor multiplication for iterative quantum time evolution of reduced density matrices. I. Theory. *J. Chem. Phys.* **102**, 4600-4610 (1995).
33. N. Makri, D. E. Makarov, Tensor multiplication for iterative quantum time evolution of reduced density matrices. II. Numerical methodology. *J. Chem. Phys.* **102**, 4611-4618 (1995).
34. N. Makri, Modular path integral: Quantum dynamics via sequential necklace linking. *J. Chem. Phys.* **148**, 101101 (2018).
35. N. Makri, Modular path integral methodology for real-time quantum dynamics. *J. Chem. Phys.* **149**, 214108 (2018).
36. S. Kundu, N. Makri, Modular path integral for discrete systems with non-diagonal couplings. *J. Chem. Phys.* **151**, 074110 (2019).
37. R. P. Feynman, Space-time approach to non-relativistic quantum mechanics. *Rev. Mod. Phys.* **20**, 367-387 (1948).
38. R. P. Feynman, A. R. Hibbs, *Quantum Mechanics and Path Integrals*. (McGraw-Hill, New York, 1965).
39. P. Nalbach, J. Eckel, M. Thorwart, Quantum coherent biomolecular energy transfer with spatially correlated fluctuations. *New Journal of Physics* **12**, 065043 (2010).
40. P. Nalbach, D. Braun, M. Thorwart, Exciton transfer dynamics and quantumness of energy transfer in the Fenna-Matthews-Olson complex. *Phys. Rev. E* **84**, 041926 (2011).

41. H.-G. Duan *et al.*, Nature does not rely on long-lived electronic quantum coherence for photosynthetic energy transfer. *Proceedings of the National Academy of Sciences*, 201702261 (2017).
42. S. Kundu, N. Makri, Real-time path integral simulation of exciton-vibration dynamics in light-harvesting bacteriochlorophyll aggregates. *J. Phys. Chem. Lett.* **11**, 8783-8789 (2020).
43. N. Makri, Small matrix disentanglement of the path integral: overcoming the exponential tensor scaling with memory length. *J. Chem. Phys.* **152**, 041104 (2020).
44. N. Makri, Small matrix path integral for system-bath dynamics. *Journal of Chemical Theory and Computation* **16**, 4038–4049 (2020).
45. N. Makri, Small matrix path integral with extended memory. *J. Chem. Theory and Comput.* **17**, 1-6 (2021).
46. S. Hess *et al.*, Femtosecond energy transfer within the LH2 peripheral antenna of the photosynthetic purple bacteria Rhodobacter sphaeroides and Rhodopseudomonas palustris LL. *Chemical Physics Letters* **216**, 247-257 (1993).
47. S. Hess *et al.*, Temporally and spectrally resolved subpicosecond energy transfer within the peripheral antenna complex (LH2) and from LH2 to the core antenna complex in photosynthetic purple bacteria. *Proc. Natl. Acad. Sci. USA* **92**, 12333-12337 (1995).
48. Y.-Z. Ma, R. J. Cogdell, T. Gillbro, Energy Transfer and Exciton Annihilation in the B800−850 Antenna Complex of the Photosynthetic Purple Bacterium Rhodopseudomonas acidophila (Strain 10050). A Femtosecond Transient Absorption Study. *The Journal of Physical Chemistry B* **101**, 1087-1095 (1997).
49. A. L. Tong *et al.*, Comparison of the Energy-Transfer Rates in Structural and Spectral Variants of the B800–850 Complex from Purple Bacteria. *The Journal of Physical Chemistry B* **124**, 1460-1469 (2020).
50. W. Humphrey, A. Dalke, K. Schulten, VMD: Visual molecular dynamics. *Journal of Molecular Graphics* **14**, 33-38 (1996).
51. S. Kundu, R. Dani, N. Makri, B800-to-B850 relaxation of excitation energy in bacterial light harvesting: All-state, all-mode path integral simulations. *J. Chem. Phys.* **157**, 115101 (2022).
52. R. Lambert, N. Makri, Quantum-classical path integral: Classical memory and weak quantum nonlocality. *J. Chem. Phys.* **137**, 22A552 (2012).
53. N. Makri, Exploiting classical decoherence in dissipative quantum dynamics: Memory, phonon emission, and the blip sum. *Chem. Phys. Lett.* **593**, 93-103 (2014).
54. N. Makri, Quantum-classical path integral: A rigorous approach to condensed phase dynamics. *International Journal of Quantum Chemistry* **115**, 1209-1214 (2015).
55. A. G. Redfield, On the theory of relaxation processes. *IBM Journal of Research and Development* **1**, 19-31 (1957).
56. T. Forster, *Ann. Phys. (Leipzig)* **2**, 55-75 (1948).
57. T. Renger, V. May, O. Kühn, Ultrafast excitation energy transfer dynamics in photosynthetic pigment–protein complexes. *Phys. Rep.* **343**, 137-254 (2001).
58. G. D. Scholes, Long-Range Resonance Energy Transfer in Molecular Systems. *Annual Review of Physical Chemistry* **54**, 57-87 (2003).
59. T. Renger, Semiclassical Modified Redfield and Generalized Förster Theories of Exciton Relaxation/Transfer in Light-Harvesting Complexes: The Quest for the Principle of Detailed Balance. *The Journal of Physical Chemistry B* **125**, 6406-6416 (2021).
60. S. Tretiak, C. Middleton, V. Chernyak, S. Mukamel, Exciton Hamiltonian for the bacteriochlorophyll system in the LH2 antenna complex of purple bacteria. *J. Phys. Chem. B* **104**, 4519-4528 (2000).

61. N. Makri, Improved Feynman propagators on a grid and non-adiabatic corrections within the path integral framework. *Chem. Phys. Lett.* **193**, 435-444 (1992).
62. N. Makri, Numerical path integral techniques for long-time quantum dynamics of dissipative systems. *J. Math. Phys.* **36**, 2430-2456 (1995).
63. R. P. Feynman, F. L. Vernon, The theory of a general quantum system interacting with a linear dissipative system. *Ann. Phys.* **24**, 118-173 (1963).

Supplementary Materials for

Tight Inner Ring Architecture and Quantum Motion of Nuclei Enable Efficient Energy Transfer in Bacterial Light Harvesting

Sohang Kundu[1], Reshmi Dani[1] and Nancy Makri[*1,2,3]

[1]*Department of Chemistry, University of Illinois, Urbana, Illinois 61801*
[2]*Department of Physics, University of Illinois, Urbana, Illinois 61801*
[3]*Illinois Quantum Information Science and Technology Center, University of Illinois, Urbana, Illinois 61801*
[*]*Corresponding Author. Email – nmakri@illinois.edu*

Spectral Density

The spectral density function $J(\omega)$ (in Figure S1a) describes the exciton-vibration coupling in each bacteriochlorophyll molecule. The two components of this spectral density i.e., the spectroscopically characterized fine structure of the 50 intramolecular vibrations, taken from Table II of Ref. (*11*), and the dissipative Ohmic bath used to model the background (*51*) are also shown in panels S1b and S1c. The Ohmic component has the functional form

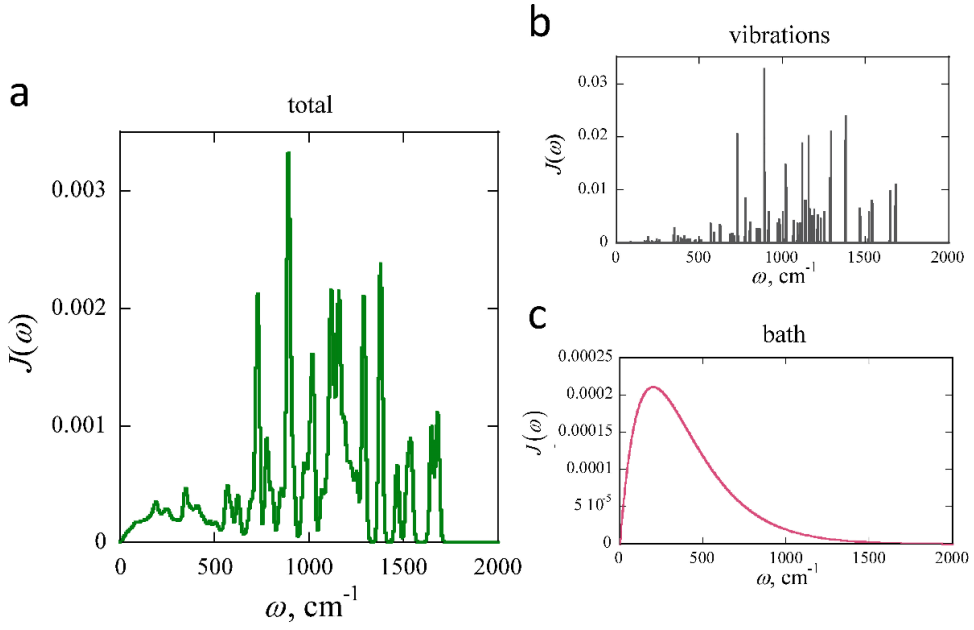

Fig. S1. Spectral density function. (a) Total spectral density used in the simulations. (b) Intramolecular component of BChl discrete normal modes. (c) Background component modeling the environment. Note the different ranges of the y-axes in atomic units.

$$J(\omega)=\frac{2\pi\hbar}{s_1^2}\xi\omega e^{-\omega/\omega_c}$$

where $\omega_c = 200\ \mathrm{cm}^{-1}$ is an exponential cutoff frequency and the Kondo parameter $\xi = 0.4$ denotes the strength of exciton-vibration coupling. The parameter s_1 is a scaling constant that sets the distances between potential minima. The reorganization energy from the intramolecular vibrations is 217 cm^{-1}, while the Ohmic background component contributes 160 cm^{-1} coming from the background, with a total equal to 377 cm^{-1}. The overall spectral profile was mildly broadened, while preserving the highly structured form and the overall reorganization energy.

While we do not average the results with respect to static disorder, we note that the background component of the spectral density contains strongly coupled modes with very low frequencies, which account to some extent to effects from inhomogeneous environments.

Video: Animation of the spatial distribution of the excitation following the initial excitation of a BChl in the B800 ring

As a supplement to this paper, we also provide a video file (screenshot shown in Figure S2) named **B800-B850.mp4** which shows the time evolution of the spatial probability distribution of the excitation energy as it transfers from the B800 to the B850 ring, over 1.5 ps.

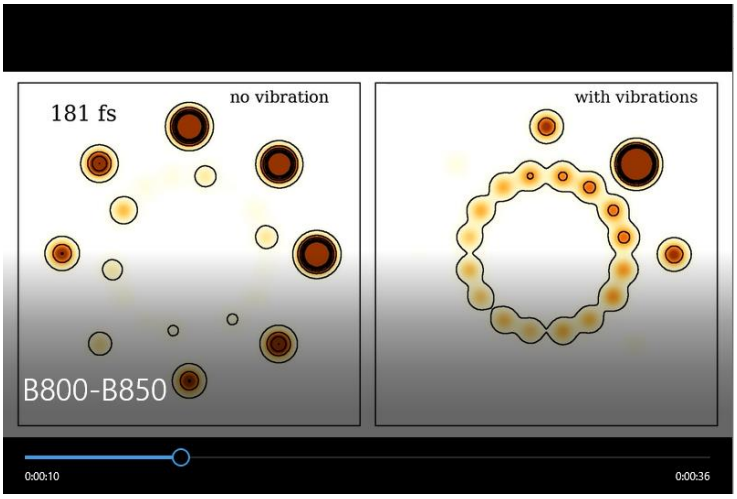

Fig S2. Video animation of the energy transfer process and snapshots. This is a screenshot taken at the 10 second mark from the video file (named B800-B850.mp4) attached as supplemental content to this paper. Snapshots from this file were used in Figures 3c and 4b.

Data Files

The data from our calculations are included in a zip file named **LH2_pathways_data_files.zip**. The contents of the folder are as follows:

- The data for Figure 2 is in six files named **FigX_with_vibrations.qda** and **FigX_without_vibrations.qda,** which include the real-time dynamics with and without the inclusion of vibrations respectively, where, X = 2a, 2b or 2c).
- All data in figure 3 can be found in the file **Fig3.qda**.
- The data in Figure 4 is in the file **Fig4.qda**, while the populations of the two rings under the classical treatment of vibrations are in the file **Fig4_classical.qda**.